



## Effective Parameter Set for Site Amplification Factors: S-wave Impedance vs. $V_{S30}$

Y. Shingaki<sup>(1)</sup>, S. Sawada<sup>(2)</sup>, H. Goto<sup>(3)</sup>

<sup>(1)</sup> Researcher, Tokyo Electric Power Services Co., Ltd., shingaki@tepsco.co.jp

<sup>(2)</sup> Professor, Kyoto University, sawada@catfish.dpri.kyoto-u.ac.jp

<sup>(3)</sup> Associate Professor, Kyoto University, goto@catfish.dpri.kyoto-u.ac.jp

### Abstract

Simplified regression models to predict the site amplification are widely adopted to seismic hazard maps, building codes, etc. In practice, the most popular parameters to control the prediction models are an averaged S-wave velocity of top  $z$  m depth,  $V_{S_z}$ , especially  $V_{S30}$ . S-wave impedance ratio of the uppermost layer to the basement,  $Z_1/Z_0$ , is alternative candidate for the prediction parameters. We compare the prediction performances for site amplification factors between  $V_{S_z}$  and  $Z_1/Z_0$ , on the basis of the numerical experiments. Depth  $z$  taking the average of S-wave velocity must be selected on the basis of the target period range of site amplification factors.  $Z_1/Z_0$  is similar performance to  $V_{S10}$ , and better than  $V_{S30}$  for PGA amplification. This implies that  $Z_1/Z_0$  is effective on the usage of site amplification predictions because  $Z_1$  only requires the physical parameter on the uppermost surface layer.

*Keywords:* site amplification, S-wave impedance,  $V_{S30}$

### 1. Introduction

Seismic waves are amplified on soft surface sediments over stiff bedrock. The amplification of ground motions closely related to earthquake damages. Prediction of the amplification at particular sites is an important issue to mitigate the damages in the field of earthquake engineering. The site amplification has been evaluated on the basis of ground motion records, especially at vertical array site, and numerical simulations considering complex subsurface structures.

Investigation of the detailed subsurface structure and precise dynamic behavior of the target soil is required to evaluate the accurate site amplification. Even if we can apply the data set at a target site, it is difficult to spatially extend the data to the surrounding area in the same order of accuracy. Therefore, the precise approach may not be adequate to the prediction in the scale of whole the earth, such as seismic hazard maps. Instead, empirical approaches are widely adopted to the prediction. Most of them are based on regression models for the site amplification factor with the arguments of a few parameters classifying the soil types. The parameters are usually estimated from the less geotechnical data. We refer to them as site parameters. The most popular one is an averaged S-wave velocity of top 30m depth,  $V_{S30}$ , and it is adopted to predict the levels of ground motion (e.g., Kanno et al., 2006 [1]; Abrahamson et al., 2014 [2]; Chiou and Youngs, 2014 [3]). S-wave impedance may be another candidate for the site parameters, because it controls a root mean square of the amplification (Goto et al., 2011 [4]).

Performance of the regression model (ground motion prediction equation, GMPE) is mainly governed by the performance of site parameters. We, thus, compare the performances between the averaged S-wave velocity and S-wave impedance on the basis of numerical experiments. In addition, conservation of normalized energy density [4] implies that S-wave impedance of only the uppermost surface layer is essential. If the performance of S-wave impedance is comparable to the averaged S-wave velocity, S-wave impedance may be the reasonable choice for the site parameter.

## 2. Averaged S-wave velocity ( $V_{S30}$ etc.)

One of the major parameters used for site classification is averaged S-wave velocity of surface ground of top  $z$  m depth, usually denoted as  $V_{S_z}$ . For a multi-layered structure model consisting of  $n$  horizontal surface layers (#1-# $n$ ) over a half-space basement (#0),  $V_{S_z}$  is defined, as follows;

$$V_{S_z} \equiv z / \sum_{i=1}^m \frac{H_i}{\beta_i}, \quad z = \sum_{i=1}^m H_i, \quad (1)$$

where  $\beta_i$  and  $H_i$  are S-wave velocity and thickness of  $i$ th layer, respectively.  $m$  is number of layers within top  $z$  m depth. The deepest layer is truncated so that sum of thickness is equal to  $z$ .

Basic concept of  $V_{S_z}$  comes from the fact that S-wave velocity of surface layers affects site amplifications (e.g., Borchardt and Gibbs, 1976 [5]; Joyner and Fumal, 1984 [6]). Borchardt et al. (1978) [7] showed negative correlation between site amplification and averaged S-wave velocity of *approximately* top 30m depth on the basis of database in San Francisco Bay region. Borchardt and Glassmoyer (1992) [8] found good correlation between amplification of peak values, e.g., peak ground acceleration (PGA), and  $V_{S30}$  from strong ground motion records during the 1989 Loma Prieta earthquake. Midorikawa (1980) [9] and Midorikawa et al. (1994) [10] also found the same correlations on the basis of database and ground motion records in Japan. Recently,  $V_{S30}$  has been the most popular parameters for site amplification, e.g., National Earthquake Hazard Reduction Program (NEHRP) and Eurocode 8. In addition, some GMPEs take into account site amplification factors by using  $V_{S30}$  (e.g., [1]; [2]; [3]).

In contrast to increasing the application of  $V_{S30}$ , some studies doubt whether  $V_{S30}$  is the best parameters to evaluate the site amplification. Wald and Mori (2000) [11] pointed out that  $V_{S30}$  showed a large variation by comparing to the observed site amplifications. Kokusho and Sato (2008) [12] revealed lower correlation between  $V_{S30}$  and site amplifications rather than  $V_{S_z}$ , whose  $z$  is evaluated from dominant period of strong ground motion records. Castellaro et al. (2008) [13] checked again the dataset of Borchardt (1994) [14] from a statistical point of view, and found no significant correlations between  $V_{S30}$  and site amplification. Gallipoli et al. (2011) [15] pointed out that the site amplification could not be estimated from  $V_{S30}$  classification because of the essential problems in the velocity inversion, which contains some ambiguity caused by intermediate rigid layers between soft soil layers (Di Giacomo et al., 2005 [16]). Some studies proposed the combination of  $V_{S30}$  and the other parameters to improve the prediction performance of  $V_{S30}$ , e.g., site period (e.g., Luzi et al., 2011 [17]; Cadet et al., 2012 [18]), depth to engineering bedrock (e.g., [2]; [3]), and variation of S-wave velocity in top 30m depth (e.g., Rathje and Navidi, 2013 [19]; Rengier et al., 2014 [20]).

We may state that 30m is not an essential depth to evaluate the site amplification by using the averaged S-wave velocity, when we integrate the past researches for both sides. Some studies discussed the prediction performance of  $V_{S10}$  (e.g., Gallipoli and Mucciarelli, 2009 [21]). In fact, Midorikawa et al. (2008) [22] pointed out that peak ground velocity (PGV) amplification was well correlated with  $V_{S30}$ , while PGA amplification was well correlated with  $V_{S10}$ . This implies that site amplifications corresponding to shorter period components are related with averaged S-wave velocities in shallower depth (smaller  $z$  values), and to longer period components are related with ones in deeper depth (larger  $z$  values). In addition, they pointed out that the relationships between  $V_{S_z}$  and site amplification factors vary due to the magnitude, i.e., frequency contents, of the earthquakes. Therefore, the depth  $z$  must be also the parameter, which depends on the selection of target indexes (PGA, PGV, etc.) and frequency contents of input ground motions. The dependency may be explained by travel time of S-wave. The travel time is evaluated from the averaged S-wave velocity and the path length. When we focus on the short (long) period components, the travel time, that is characteristic time for the system, must be small (large).

Site amplification is mainly controlled by the impedance contrast. The value of  $V_{S_z}$  aims to account for the contrast. On the other hand, the selection of depth  $z$  aims to find an effective depth corresponding to the target period range. When we distinguish each contribution to site amplification, the factor is not required to be the averaged S-wave velocity.

### 3. S-wave impedance ratio

S-wave impedance is defined by multiplying S-wave velocity and density. Its ratio between surface layers and basement controls the peak value of transfer function of surface ground. Therefore, some researches focused on the relation between the S-wave impedance ratio and site amplification. Shima (1978) [23] pointed out that S-wave velocity ratio between the uppermost layer and the basement is well correlated with the site amplifications by carrying out numerical simulations. Joyner et al. (1981) [24] proposed the square root of ratio between the averaged S-wave impedance of near surface and the basement as appropriate parameter of the site amplification. Boore (2013) [25] introduced the same S-wave impedance ratio to approximately compute the site amplification, namely SRI method. Joyner et al. (1981), Boore (2013) and the other studies (e.g., Boore, 2003 [26]) take the average over a depth defined by the target frequency for the S-wave impedance of near surface.

Some researchers (e.g., [24]; [25]) referred to ray theory in order to explain the reason why they applied the S-wave impedance ratio to estimate the site amplification, although the ray theory is not available in case of wave propagation in the multi-layered structures [4]. Another theoretical background is available in terms of normalized energy density (NED), which was proposed by Goto et al. (2011). NED is defined by a following form when SH wave vertically transmits to multi-layered structures (Goto et al., 2013 [27]);

$$\text{NED}_i \equiv \lim_{\Omega \rightarrow \infty} \frac{1}{\Omega} \int_0^{\Omega} \rho_i \beta_i \left| \frac{A_i(\omega)}{A_0(\omega)} \right|^2 d\omega, \quad (2)$$

where  $A_0$  is a Fourier amplitude of the incident wave, and  $A_i$  is a Fourier amplitude of the upgoing wave in the  $i$ th layer.  $\rho_i$  is the density of  $i$ th layer, and  $\omega$  is the angular frequency. NED is a product of frequency-averaged power of transfer function and S-wave impedance  $Z_i$ , which is defined by  $\rho_i \beta_i$ . Goto et al. (2011) established an essential principle of NED; NED is constant over the all layers ( $\text{NED}_i = \text{NED}_0 = \rho_0 \beta_0$ ) even if any velocity contrasts exist in the multi-layered structure.

On the basis of the principle, root mean square (RMS) of the upgoing wave amplification in the uppermost layer ( $i=1$ ) is derived, as follows;

$$\sqrt{\lim_{\Omega \rightarrow \infty} \frac{1}{\Omega} \int_0^{\Omega} \left| \frac{A_1(\omega)}{A_0(\omega)} \right|^2 d\omega} = \sqrt{\frac{\rho_0 \beta_0}{\rho_1 \beta_1}} \equiv \sqrt{\frac{Z_0}{Z_1}}, \quad (3)$$

where  $Z_1/Z_0$  is a S-wave impedance ratio of the uppermost layer to the basement. From Eq. (3), RMS of transfer function between ground surface and basement is proportional to the inverse square root of the S-wave impedance ratio ( $Z_1/Z_0$ ). In addition, the ratio also controls the peak value of the transfer function. Day (1996) [28] derived the same result about the downgoing wave amplification. He also pointed out that the RMS of transfer function over the finite bandwidth of  $\omega$  does not depend on the ground structure below the depth defined by the bandwidth. Therefore,  $Z_1/Z_0$  is another candidate to represent the site amplification. Note that no information of intermediate layers is required to evaluate the value of  $Z_1/Z_0$ . Only the S-wave impedance of the uppermost layer needs to be estimated when the reference basement is defined. Recently, Goto et al. (2015) [29] proposed a measurement method of the S-wave impedance of the uppermost layer. The method requires only to touch the ground surface, and not to disturb the ground environment, such as boring.

## 4. Numerical experiments

### 4.1 Method and model

In this article, we adopt  $V_{S30}$ ,  $V_{S10}$ , and  $Z_1/Z_0$  as indexes to characterize the site amplifications, namely site parameters. Monte Carlo simulations are performed by assuming vertical propagation of SH wave through 1D hypothetical stratified layers whose all geotechnical data are known, and the relationship between site amplification factors and the site parameters is discussed on the basis of the simulation results.

Total site amplifications are controlled by the subsurface structure above the seismological bedrock (~2000-3000m/s of S-wave velocity), which is located in the order of 1-3km depth in Tokyo and Osaka areas in Japan. On the other hand, the effective periods of the subsurface structure are longer period components (5-12s), which is not our target period range. For example, the dominant periods of the severe ground motion damage observed in Osaki city and Namie town during the 2011 Tohoku earthquake in Japan are estimated around 0.3-0.6s, and the site amplification can be explained by very shallow structure (e.g., Goto and Midorikawa, 2012 [30]; Goto et al., 2012 [31]; Goto et al., 2016 [32]). In addition, the total site amplifications cannot be discussed under the assumption of both 1D stratified media and vertical incident of S-wave. In practice, the amplification due to the deep subsurface structure must be estimated from the detailed 3D subsurface structure by using 3D precise numerical simulations, and/or site amplification factors estimated from ground motion records by spectral inversion methods. In one example, any (single) site parameters cannot explain the basin edge effect occurred in 1995 Kobe earthquake (e.g., Kawase, 1996 [33]). Therefore, we focus on the shallower stiff layer called “engineering bedrock” as the basement. It is usually defined by 300-700m/s of S-wave velocity.

We randomly create three-layered structures consisting of 2 horizontal surface layers (#1 and #2) over the half space basement (#0), as shown in Fig.1. Each medium assumes to be linear elastic material. No damping is assumed in the basement, and damping coefficients are introduced into each surface layer by using complex stiffness. Physical values of the basement, 600m/s for S-wave velocity and 2200kg/m<sup>3</sup> for density, are common in all the cases. 10,000 models are generated by sampling each physical value of the surface layers in a range of 100-600m/s for S-wave velocity, 1500-2200kg/m<sup>3</sup> for density and 0.01-0.05 for damping coefficient. In order to enhance the soft sediment cases, an additional parameter  $x$  is uniformly sampled from log100 to log600, and the S-wave velocity is calculated from a value of  $10^x$ . The other parameters are uniformly sampled from the range. If the S-wave impedance of the surface layer #1 is larger than that of the layer #2, the parameters are exchanged. It ensures softer layer allocated on the uppermost layer. Total thickness of the surface layers is sampled from uniform distribution in a range of 10-100m, and the interface between the surface layer #1 and #2 is also randomly selected. Histograms of the three site parameters and the total thickness are shown in Fig.2.

Responses on free surface of the three-layered structure models are numerically computed by using Haskell-Thomson method (Thomson, 1950 [34]; Haskell, 1953 [35]). The frequency range of the simulation is lower than or equal to 50Hz. We assume to keep linear elastic response in this simulation. In practice, nonlinear soil response is effective under the strong ground motions, and it should be considered in site amplification predictions (e.g., Seyhan and Stewart, 2014 [36]). On the other hand, the final execution of equivalent linear analysis, e.g., SHAKE (Schnabel et al., 1972 [37]), is linear elastic response with the corresponding shear modulus to shear strains. In this simulation, the parameter sets include the cases of shear modulus degradation.

The calculated transfer functions,  $|2A_1| / |2A_0|$ , for all the generated models are shown in Fig.3. Site amplification factor is defined by a ratio of calculated values to values in case of homogeneous model whose physical parameter is the same with the basement. In the article, peak ground acceleration (PGA) and peak ground velocity (PGV) are adopted to calculate the factors.

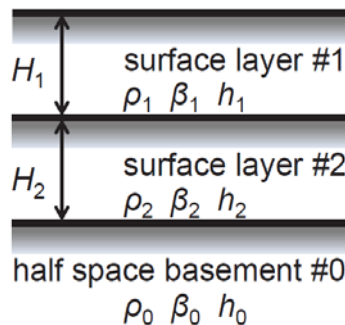


Fig. 1 – Structure model for Monte Carlo simulations, consisting of two surface layers and a half-space basement.  $\beta_i$ ,  $\rho_i$ ,  $h_i$  and  $H_i$  are S-wave velocity, density, damping coefficient and the thickness of  $i$ th layer, respectively. Physical values of basement are common to all the models,  $\beta_0 = 600$  (m/s),  $\rho_0 = 2200$  (kg/m<sup>3</sup>),  $h_0 = 0$ . S-wave impedances are ensured to be the ascending order  $\rho_1\beta_1 < \rho_2\beta_2 < \rho_0\beta_0$ .

We apply three types of incident waves, whose 5% damped acceleration spectra and time histories of acceleration are shown in Fig.4. Type A, Type B, and Type C waves enhance short, middle, and long period components, respectively. Ratios of 5% damped acceleration spectra in 0.1-1.0s are listed in Table 1. The peak periods of 5% damped acceleration and velocity spectra of the three waves are also listed in the same table.

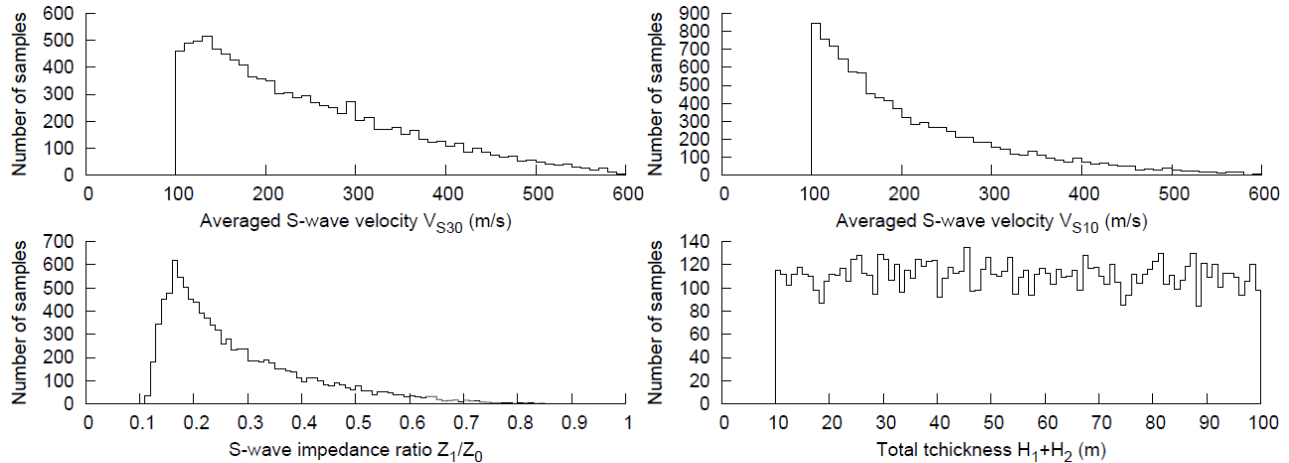


Fig. 2 – Histograms of the three site parameters and total thickness of the 10,000 models. (a) averaged S-wave velocity to 30m depth;  $V_{S30}$ . (b) averaged S-wave velocity to 10m depth;  $V_{S10}$ . (c) S-wave impedance ratio between the uppermost layer and the basement;  $Z_1/Z_0$ . (d) Total thickness;  $H_1+H_2$ .

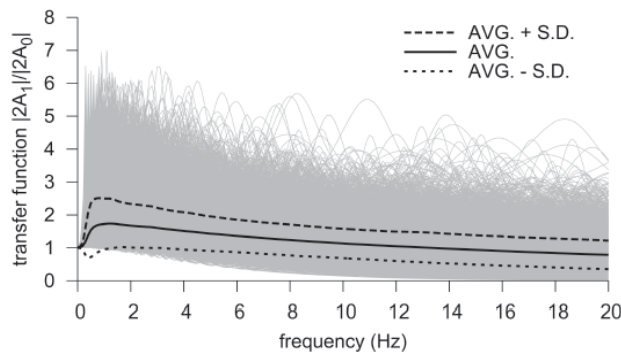


Fig. 3 – The transfer functions between ground surface and basement  $|2A_1| / |2A_0|$  for randomly generated 10,000 models. The gray solid line plots all the transfer functions for each model. The black solid line is its average, and the black dashed lines are the range of standard deviation from the average value.

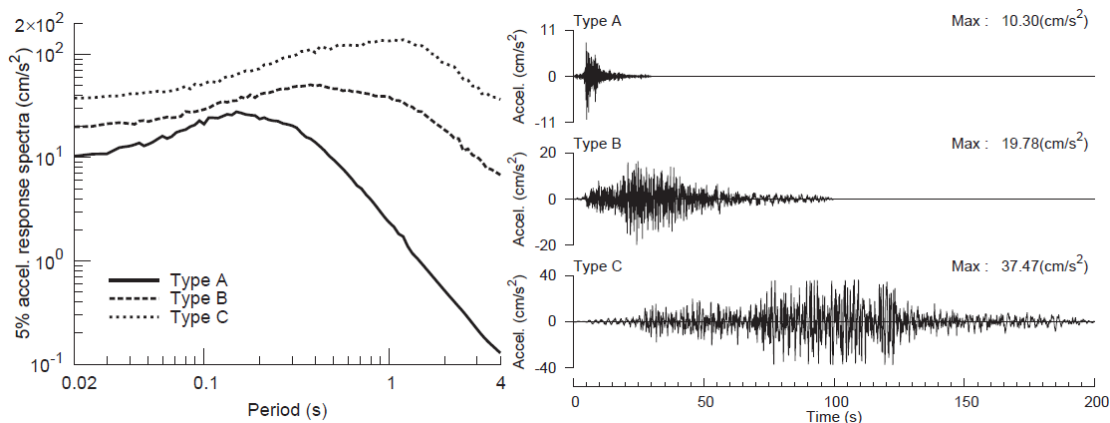


Fig. 4 – Three types of incident waves. (a) 5% damped acceleration spectra. (b) Time history of acceleration. Type A, Type B, and Type C enhance short, middle, and long period components, respectively.

Table 1 – Characteristics of the three incident waves. Ratios of 5% damped spectral acceleration values between 0.1s and 1.0s are listed in 2nd column. The peak periods of 5% damped acceleration spectra and velocity spectra are listed in 3rd and 4th column, respectively.

Incident wave	1.0s spectral acceleration / 0.1s spectral acceleration	Peak period of 5% damped response spectra (s)	
		Acceleration ( $T_{max}^{Sa}$ )	Velocity ( $T_{max}^{Sv}$ )
Type A (short)	0.11	0.15	0.27
Type B (middle)	1.31	0.35	1.30
Type C (long)	2.59	1.08	2.18

#### 4.2 Correlation between site parameter and site amplification factor

Fig.5 shows 5% damped acceleration response spectra on ground surface for each incident wave, Type A-C. In comparison to the response spectra of incident waves, the spectra keep some frequency contents of incident waves, although they vary due to the variation of site amplifications. Note that some response spectra in short period components up to 0.5s are less than ones for input waves, especially for Type A cases. Amount of internal damping may affect the attenuation.

Fig.6 and Fig.7 show the relationships between site parameters and site amplification factors for each incident wave. Each of them consists of 9 figures that is a combination of three site parameters and three types of incident wave. Fig.6 and Fig.7 show the results for two site amplification factors; PGA amplification and PGV amplification, respectively. Table 2 lists the correlation coefficients between each site parameter and all the site amplification factors including all types of incident waves, and Table 3 lists the correlation coefficients between all the combination of site parameters and site amplification factors.

As  $V_{S30}$  increases, all the site amplification factors do not monotonically decrease for the incident wave of Type A (short-period wave). Positive correlation between the factors and  $V_{S30}$  appears well in 100-200m/s of  $V_{S30}$ . This feature is also seen for the other incident waves in the cases of PGA amplification. It seems to be in opposite sense if  $V_{S30}$  represents well the site amplifications. Aboye et al. (2015) [38] also pointed out the feature. The results are relatively improved in cases of  $V_{S10}$ . On the other hand,  $V_{S30}$  is highly correlated with site amplification factors for the incident wave of Type B (middle-period wave) and C (long-period wave), especially in cases of PGV amplification, as shown in Table 3. PGA amplification is the factor essentially focusing on the short-period amplifications, while PGV amplification is focusing on middle- to long-period amplifications. Therefore,  $V_{S30}$  is a better selection as the site parameter than  $V_{S10}$  when we focus on the middle- to long-period

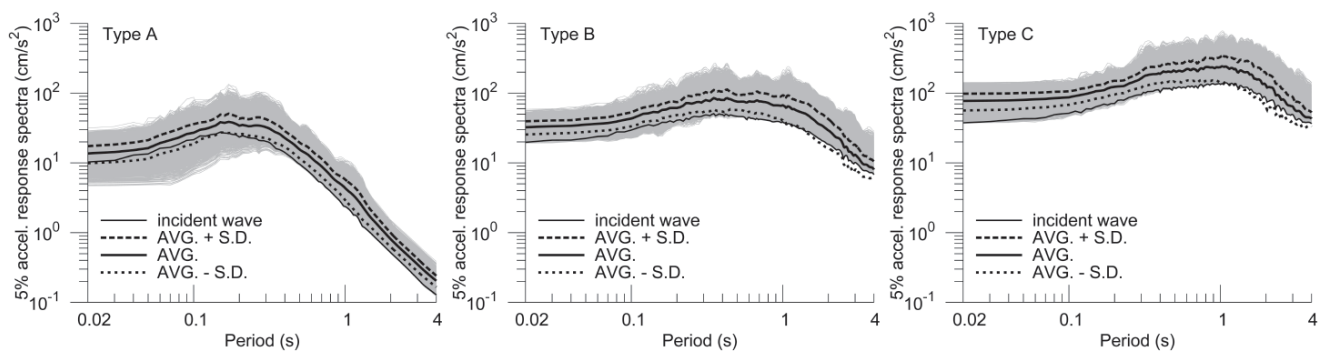


Fig. 5 – The 5% damped acceleration response spectra on the ground surface. Types of incident waves, Type A, B, and C, are tiled in left, middle, and right columns, respectively. Each gray solid line is a calculated result corresponding to one of the randomly generated 10,000 models. The black broken lines and the black solid lines are the range of standard deviations and average values of the results. The thin lines are ones for incident waves.

amplifications, and vice versa for short-period amplifications. It is consistent with the results by Midorikawa et al. (2008). Depth  $z$  of the averaged S-wave velocity should be selected in a manner of period range for the target site amplification factors.

As  $Z_1/Z_0$  increases, most of the site amplification factors monotonically decrease. The feature does not depend on the types of incident waves and the site amplification factors. Overall correlation coefficients (Table 2) for  $Z_1/Z_0$  are not significantly different with both  $V_{S10}$  and  $V_{S30}$ , while the correlations are better in cases for PGA amplification and/or short period wave (Type A) as similar to  $V_{S10}$ .  $Z_1/Z_0$  only uses material parameter on uppermost surface layer when the reference basement is defined. Therefore,  $Z_1/Z_0$  may be alternative to  $V_{S10}$  if we have no information about velocity profiles to 10m depth. In Fig.6 and Fig.7, curves of inverse square root of  $Z_1/Z_0$  are plotted together with the results. The upper bound of the site amplification factors is close to the inverse square root of  $Z_1/Z_0$  for most of the results. Only for PGA amplification and Type C incident wave, the geometric mean of the factors is very close to the curve. The lower bound of the factors is close to 1 regardless of the values of  $Z_1/Z_0$  for most of the results. It implies that the upper and lower bounds seem to be systematically determined.

Site Amplification Factor : Peak Ground Acceleration (PGA)

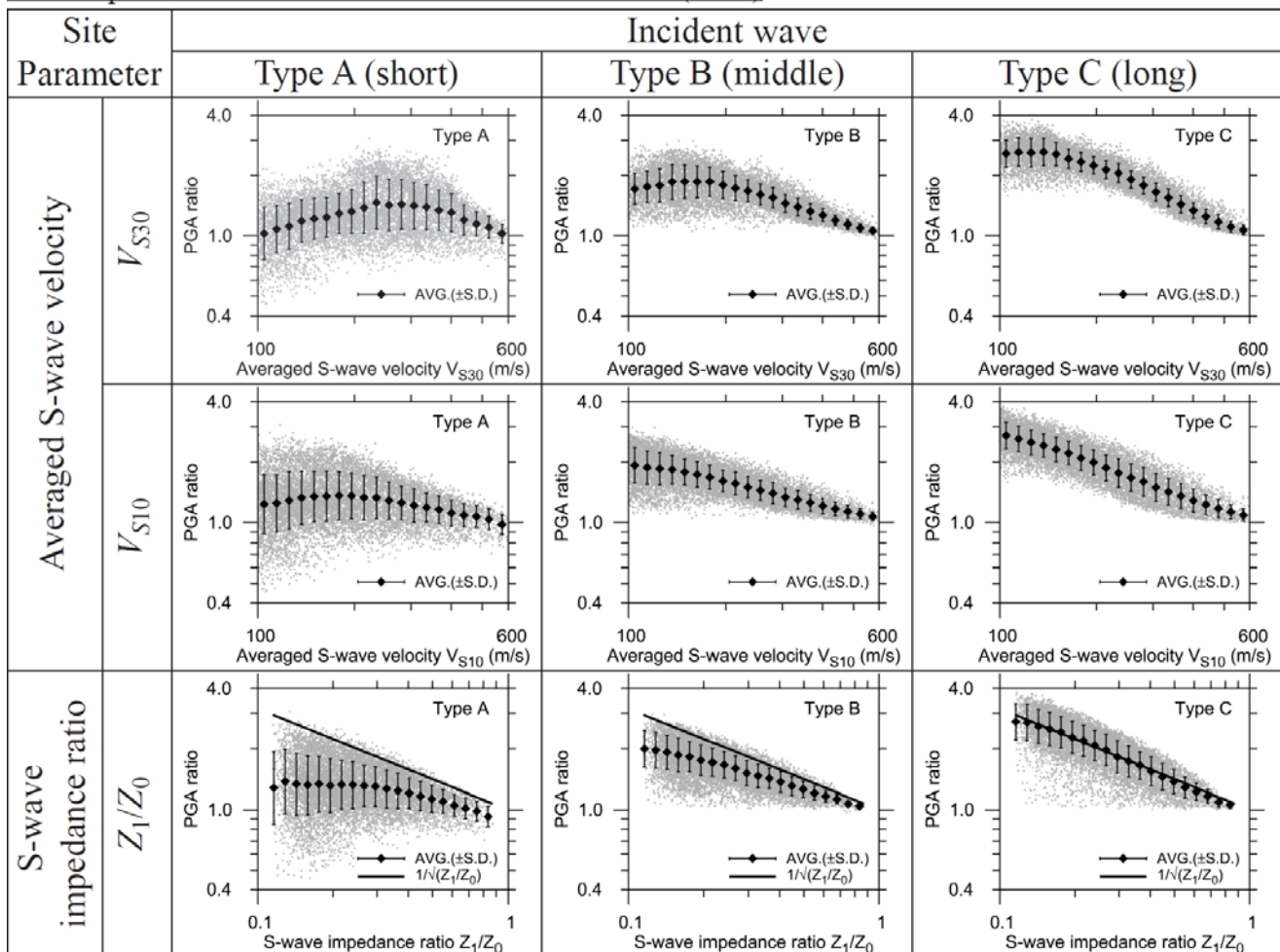


Fig. 6 – Scatter plots between site parameter and peak ground acceleration (PGA). Types of incident waves, type A, B, and C, are tiled in left, middle, and right columns, respectively. Each vertical axis is amplification of PGA. Horizontal axes are site parameters,  $V_{S30}$ ,  $V_{S10}$ , and  $Z_1/Z_0$ , from top to bottom rows, respectively. Each gray dot is a calculated result corresponding to one of the randomly generated 10,000 models. Error bars and the center symbols are the range of standard deviations and mean values of the results. The black solid line in the figures related to S-wave impedance ratio represents a curve of inverse square root of S-wave impedance ratio.

### 4.3 Prediction equation for site amplification factor

As shown in Table 3, the correlation coefficient for PGA amplification and Type A is lowest. This implies that the site amplification factors for short period components may be also controlled by the amount of internal damping.  $V_{S_z}$  and  $Z_1/Z_0$  are satisfied only for no damping cases. Site amplification factors for models with damping must be less than those without damping. Anderson et al. (1996) [39] proposed to adopt an average property of attenuation in multi-layers. The parameter was named a total damping  $t_S^*$  by Goto et al. (2013), and defined, as follows;

$$t_S^* = \sum_{i=1}^n \frac{2H_i h_i}{\beta_i}, \quad (4)$$

where  $h_i$  is damping coefficient of  $i$ th layer. Anderson et al. (1996) found that site classification using both the averaged S-wave velocity and  $t_S^*$  allows accurate prediction of peak and RMS accelerations. Goto et al. (2013) pointed out that NED is not constant over the layers if the material contains the intrinsic damping, and decay of

Site Amplification Factor : Peak Ground Velocity (PGV)

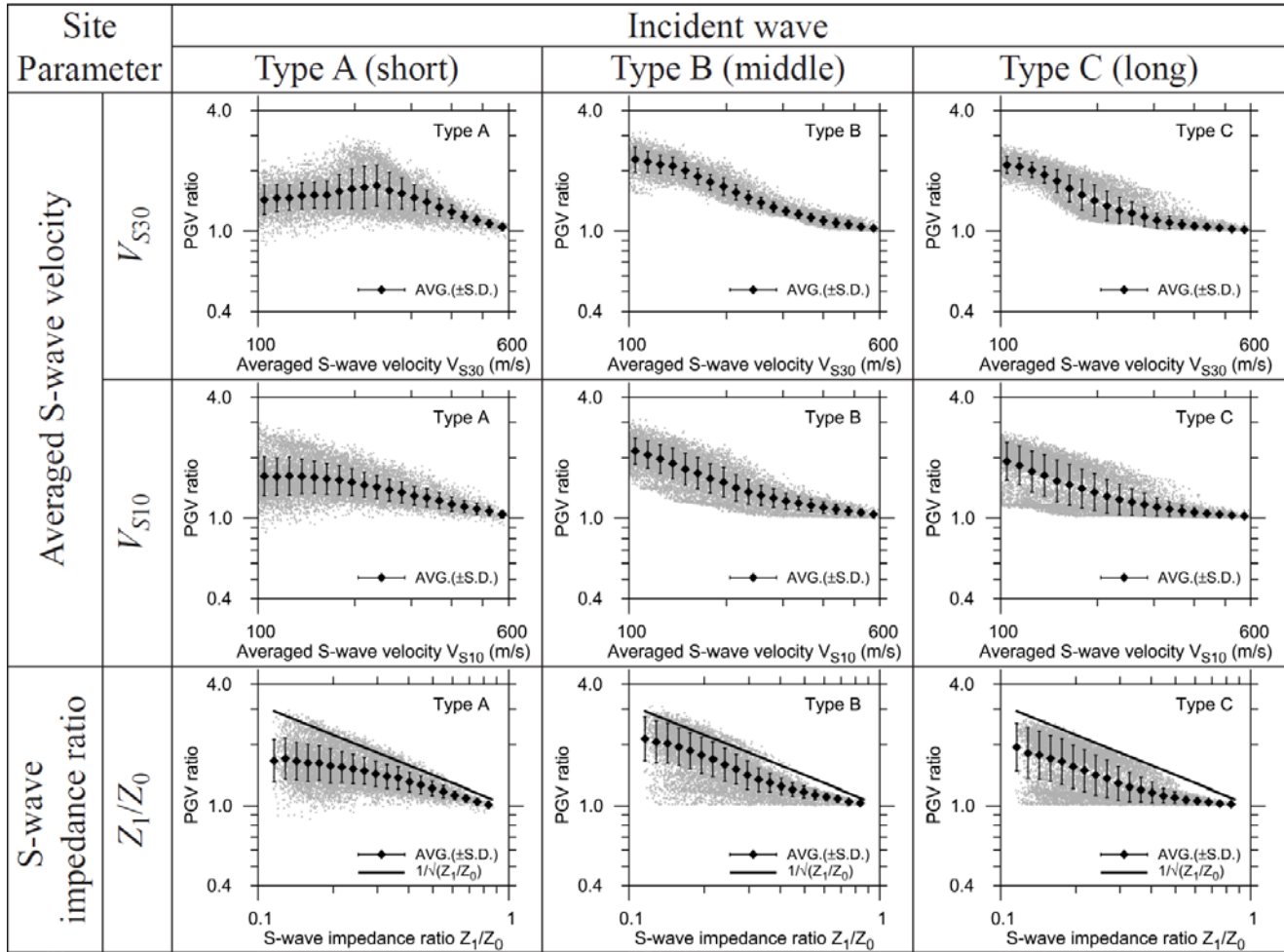


Fig. 7 – Scatter plots between site parameter and peak ground velocity (PGV). Types of incident waves, type A, B, and C, are tiled in left, middle, and right columns, respectively. Each vertical axis is amplification of PGV. Horizontal axes are site parameters,  $V_{S30}$ ,  $V_{S10}$ , and  $Z_1/Z_0$ , from top to bottom rows, respectively. Each gray dot is a calculated result corresponding to one of the randomly generated 10,000 models. Error bars and the center symbols are the range of standard deviations and mean values of the results. The black solid line in the figures related to S-wave impedance ratio represents a curve of inverse square root of S-wave impedance ratio.

Table 2 – Correlation coefficients between site parameters and site amplification factors for all combinations of incident wave types and site amplification factors.

Site parameters	$V_{S30}$	$V_{S10}$	$Z_1/Z_0$
Correlation coefficients	-0.514	-0.549	-0.523

Table 3 – Correlation coefficients between site parameters and site amplification factors.

Site amplification factors		PGA ratio			PGV ratio		
Incident wave		Type A	Type B	Type C	Type A	Type B	Type C
Site parameters	$V_{S30}$	0.174	-0.652	-0.888	-0.299	-0.941	-0.874
	$V_{S10}$	-0.135	-0.728	-0.863	-0.542	-0.820	-0.687
	$Z_1/Z_0$	-0.220	-0.694	-0.792	-0.545	-0.739	-0.612

NED values is well correlated with  $t_S^*$ . Therefore, the variation containing in the results for short period cases may be reduced when we adopt the additional parameter  $t_S^*$ . We evaluate a prediction equation for site amplification factor in a function of site parameter  $V_{S_z}$  or  $Z_1/Z_0$ , and the total damping  $t_S^*$ . Let  $A$  be a site amplification factor (i.e., PGA amplification and PGV amplification), and the prediction equation is proposed, as follows:

$$\ln A = c_0 + c_1 \ln S - \pi \frac{t_S^*}{T_{\max}} \quad (5)$$

where  $S$  is defined by a relative value of site parameters;  $V_{S_z}/\beta_0$  for the averaged S-wave velocity, and  $Z_1/Z_0$  for the impedance ratio.  $c_0$  and  $c_1$  are regression coefficients that are estimated from results for all the combination of 10,000 models and 3 types of incident waves. The third term represents the explicit contribution of the total damping. Amplitude decay of seismic wave due to the internal damping and scatterings is generally modeled by an exponential function of frequency (e.g., [39]). In this article, the variable of the function is substituted with an effective frequency of incident waves, which are defined by an inverse of peak periods of their response spectra ( $T_{\max}$ ). Peak periods of 5% damped acceleration spectra and velocity spectra for the incident wave are adopted to PGA prediction and PGV prediction, respectively. The former is denoted by  $T_{\max}^{Sa}$ , and the latter is denoted by  $T_{\max}^{Sv}$ , whose values are listed in Table 1.

Table 4 shows the estimated regression coefficients for PGA amplification and PGV amplification, and RMS residuals from the predicted values.  $V_{S10}$  is the best parameters for PGA prediction, and  $V_{S30}$  is the best parameters for PGV prediction in terms of RMS residuals. On the other hand, regression coefficient  $c_0$  of  $Z_1/Z_0$  for PGA prediction is almost zero. It means that the site amplification factor for PGA may be essentially represented by  $Z_1/Z_0$  and  $t_S^*$ . In fact, RMS residual for  $Z_1/Z_0$  (0.170) is smaller than one for  $V_{S30}$  (0.185) when the coefficient  $c_0$  constrains to be zero in case of PGA prediction.

For prediction equation, statistical independence of the arguments should be clarified. Correlation coefficient between  $t_S^*$  and  $Z_1/Z_0$  is estimated as -0.35 on the basis of the same samples in estimating the prediction equation. On the other hand, correlation coefficients between  $t_S^*$  and  $V_{S30}$ , and between  $t_S^*$  and  $V_{S10}$  are -0.60 and -0.44, respectively. The large correlation coefficients for the averaged S-wave velocity are expected from the definition of  $t_S^*$  by reference to Eq. (1) and (4). A set of independent arguments  $t_S^*$  and  $Z_1/Z_0$  will give a good PGA prediction from statistical point of view.

Table 4 – Regression coefficients of prediction equation for site amplification factor, and RMS residuals from the predicted values.

S	PGA ratio			PGV ratio		
	$c_0$	$c_1$	RMS	$c_0$	$c_1$	RMS
$V_{S30}/\beta_0$	0.188	-0.442	0.169	-0.025	-0.494	0.159
$V_{S10}/\beta_0$	0.086	-0.478	0.157	-0.054	-0.459	0.185
$Z_1/Z_0$	0.004	-0.456	0.170	-0.108	-0.420	0.202

## 5. Conclusions and remarks

We compare the prediction performances for site amplification factors between the averaged S-wave velocity  $V_{S_z}$ , and S-wave impedance ratio  $Z_1/Z_0$ . On the basis of the numerical experiments assuming vertical propagation of SH wave through 1D stratified layers, we estimate correlation coefficients between the site parameters and the site amplification factors, and errors from prediction equations.

$V_{S30}$  is more highly correlated with the middle- to long-period site amplification factors such as PGV amplification for the middle- to long-period incident waves than  $V_{S10}$  and  $Z_1/Z_0$ . On the other hand, when we focus on the short-period site amplification factors such as PGA amplification or cases for incident wave of Type A (short-period wave), the factors does not monotonically decrease as  $V_{S30}$  increases. This indicates that the largest site amplification factors should be predicted at a particular value of  $V_{S30}$ . In contrast,  $V_{S10}$  almost shows the monotonic decrease. Although  $V_{S_z}$  aims to account for the impedance contrast to the bedrock, the selection of depth  $z$  must depend on the target period range.  $Z_1/Z_0$  also shows the monotonic relationship with site amplification factors regardless of the target period range. In addition, the upper bound of the site amplification factors is close to the inverse square of  $Z_1/Z_0$  and the lower one is close to 1 regardless the value of  $Z_1/Z_0$  for most of the results.  $Z_1/Z_0$  shows the similar correlation coefficients to  $V_{S10}$  in cases for the short-period site amplification factors and for incident wave of Type A (short-period wave).

From the results of numerical experiments, we can conclude that  $Z_1/Z_0$  is similar performance to  $V_{S10}$  for the short-period components, i.e., short-period site amplification factors or incident wave enhancing short-period components. In order to evaluate  $V_{S_z}$ , precise information about the subsurface structure of top  $z$  m depth is required by using PS loggings. The investigation takes a large cost, and thus the values of  $V_{S_z}$  are usually estimated from geomorphologic classifications (e.g., Wakamatsu and Matsuoka, 2006 [40]), and topographic data (e.g., Wald and Allen, 2007 [41]). Therefore,  $V_{S_z}$  itself contains some estimation error. On the other hand,  $Z_1/Z_0$  only requires S-wave impedance of the uppermost surface layer when the reference basement is defined. The measurement technique of the S-wave impedance without any disturbances of ground has been proposed by Goto et al. (2015), which the instruments only touch the ground surface. This implies that the estimate performance of  $Z_1/Z_0$  itself is better than  $V_{S_z}$ . Therefore, the prediction equation based on the  $Z_1/Z_0$  might be effective.

## 6. Acknowledgements

We used the strong motion records of K-NET provided by National Research Institute for Earth Science and Disaster Prevention in Japan as a reference for the phase characteristics of the synthetic seismic waves. We are grateful to the organization.

## 7. References

- [1] Kanno T, Narita A, Morikawa N, Fujiwara H, Fukushima Y (2006): A new attenuation relation for strong ground motion in Japan based on recorded data. *Bull. Seismol. Soc. Am.*, **96** (3), 879-897.

- [2] Abrahamson NA, Silva WJ, Kamai R (2014): Summary of the ASK14 ground motion relation for active crustal regions. *Earthq. Spectra*, **30** (3), 1025–1055.
- [3] Chiou BS-J, Youngs RR (2014): Update of the Chiou and Youngs NGA model for the average horizontal component of peak ground motion and response spectra. *Earthq. Spectra*, **30** (3), 1117–1153.
- [4] Goto H, Sawada S, Hirai T (2011): Conserved quantity of elastic waves in multi-layered media: 2D SH case - Normalized Energy Density-. *Soils and Foundations*, **55** (5), 1282-1292.
- [5] Borcherdt RD, Gibbs JF (1976): Effects of local geological conditions in the San Francisco bay region on ground motions and the intensities of the 1906 earthquake. *Bull. Seismol. Soc. Am.*, **66** (2), 467-500.
- [6] Joyner WB, Fumal TE (1984): Use of measured shear-wave velocity for predicting geologic and site effects on strong ground motion. *8<sup>th</sup> World Conference on Earthquake Engineering 8WCEE*, San Francisco, USA, **2**, 777-783.
- [7] Borcherdt RD, Gibbs JF, Fumal TE (1978): Progress on ground motion predictions for the San Francisco Bay region, California. *2<sup>nd</sup> international conference on microzonation*, San Francisco, USA, **1**, 241-253.
- [8] Borcherdt RD, Glassmoyer G (1992): On the characteristics of local geology and their influence on ground motions generated by the Loma Prieta earthquake in the San Francisco Bay region, California. *Bull. Seismol. Soc. Am.*, **82** (2), 603-641.
- [9] Midorikawa S (1980): Estimation of peak ground acceleration and velocity with regard to fault rupture and site condition. *8<sup>th</sup> Symposium on Ground Vibrations*, Tokyo, Japan, 56-64 (in Japanese).
- [10] Midorikawa S, Matsuoka M, Sakugawa K (1994): Site effects on strong-motion records observed during the 1987 Chiba-Ken-Toho-Okai. Japan Earthquake, *9<sup>th</sup> Japan Earthquake Engineering Symposium*, Tokyo, Japan, **3**, 85-90.
- [11] Wald LA, Mori J (2000): Evaluation of methods for estimating linear site-response amplifications in the Los Angeles Region. *Bull. Seismol. Soc. Am.*, **90** (6B), S32-S42.
- [12] Kokusho T, Sato K (2008): Surface-to-base amplification evaluated from KiK-net vertical array strong motion records. *Soil Dyn. Earthq. Eng.*, **28**, 707–716.
- [13] Castellaro S, Mulargia F, Rossi PM (2008): Vs30: Proxy for seismic amplification?. *Seismol. Res. Lett.*, **79** (4), 540-543.
- [14] Borcherdt RD (1994): Estimates of site-dependent response spectra for design (methodology and justification). *Earthq. Spectra*, **10** (4), 617-653.
- [15] Gallipoli MR, Albarello D, Mucciarelli M, Bianca M (2011): Ambient noise measurements to support emergency seismic microzonation: the Abruzzo 2009 earthquake experience. *Bollettino di Geofisica Teorica ed Applicata*, **52** (3), 530-559.
- [16] Di Giacomo D, Gallipoli MR, Mucciarelli M, Parolai S, Richwalski SM (2005): Analysis and modeling of HVSR in the presence of a velocity inversion: the case of Venosa, Italy. *Bull. Seismol. Soc. Am.*, **95** (6), 2364-2372.
- [17] Luzi L, Puglia R, Pacor F, Gallipoli MR, Bindi D, Mucciarelli M (2011): Proposal for a soil classification based on parameters alternative or complementary to  $V_{s,30}$ . *Bull. Earthq. Eng.*, **9** (6), 1877-1898.
- [18] Cadet H, Bird P-Y, Duval A-M, Bertrand E (2012): Site effect assessment using KiK-net data: Part 2- Site amplification prediction equation based on  $f_0$  and  $V_{sz}$ . *Bull. Earthq. Eng.*, **10** (2), 451-489.
- [19] Rathje EM, Navidi S (2013): Identification of Site Parameters that Improve Predictions of Site Amplification. *Technical Report PEER 2013/18*, Pacific Earthquake Engineering Research, Berkeley, USA.
- [20] Rengier J, Bonilla LF, Bertrand E, Semblat J-F (2014): Influence of the  $V_s$  beyond 30m depth on linear site effects: Assessment from the KiK-net data. *Bull. Seismol. Soc. Am.*, **104** (5), 2337-2348.
- [21] Gallipoli MR, Mucciarelli M (2009): Comparison of site classification from  $V_{s30}$ ,  $V_{s10}$ , and HVSR in Italy. *Bull. Seismol. Soc. Am.*, **99** (1), 340-351.
- [22] Midorikawa S, Komazawa M, Miura H (2008): Relationships between average shear-wave velocity and site amplification factors obtained by records from Yokohama dense strong-motion network. *Journal of JAEE*, **8** (3), 19-30 (in Japanese with English abstract).
- [23] Shima E (1978): Seismic microzoning map of Tokyo. *2<sup>nd</sup> international conference on microzonation*, San Francisco, USA, **1**, 433-443.

- [24] Joyner WB, Warrick RE, Fumal TE (1981): The effect of quaternary alluvium on strong ground motion in the Coyote Lake, California, earthquake of 1979. *Bull. Seismol. Soc. Am.*, **71** (4), 1333-1349.
- [25] Boore DM (2013): The uses and limitations of the Square-Root-Impedance method for computing site amplification. *Bull. Seismol. Soc. Am.*, **103** (4), 2356-2368.
- [26] Boore DM (2003): Simulation of ground motion using the stochastic method. *Pure and Applied Geophysics*, **160**, 635-676.
- [27] Goto H, Kawamura Y, Sawada S, Akazawa T (2013): Direct estimation of near-surface damping based on normalized energy density. *Geophys. J. Int.*, **194** (1), 488-498.
- [28] Day SM (1996): RMS response of a one-dimensional half-space to SH. *Bull. Seismol. Soc. Am.*, **86** (2), 363-370.
- [29] Goto H, Tanaka N, Sawada S, Inatani H (2015): S-wave impedance measurements of the uppermost material in surface ground layers. *Soils and Foundations*, **55** (5), 1282-1292.
- [30] Goto H, Morikawa H (2012): Ground motion characteristics during the 2011 off the Pacific coast of Tohoku earthquake. *Soils and Foundations*, **52** (5), 769-779.
- [31] Goto H, Morikawa H, Inatani M, Ogura Y, Tokue S, Zhang X-R, Iwasaki M, Araki M, Sawada S, Zerva A (2012): Very dense seismic array observations in Furukawa district, Japan. *Seismol. Res. Lett.*, **83** (5), 765-774.
- [32] Goto H, Hada K, Sawada S, Yoshida N, Ouchi T (2016): Evaluation of site response on downtown area of Namie town, Fukushima, based on microtremor and aftershock observations. *Journal of JAEE*, **16** (1), 309-321 (in Japanese with English abstract).
- [33] Kawase H (1996): The cause of the damage belt in Kobe: "the basin-edge effect," constructive interference of the direct S-wave with the basin-induced diffracted/Rayleigh waves. *Seismol. Res. Lett.*, **67** (5), 25-34.
- [34] Thomson W (1950): Transmission of elastic waves through a stratified solid. *J. Appl. Phys.*, **21**, 89-93.
- [35] Haskell N (1953): The dispersion of surface waves in multilayered media. *Bull. Seismol. Soc. Am.*, **43** (1), 17-34.
- [36] Seyhan E, Stewart JP (2014): Semi-empirical nonlinear site amplification from NGA-West 2 data and simulations. *Earthq. Spectra*, **30** (3), 1241-1256.
- [37] Schnabel PB, Lysmer J, Seed HB (1972): SHAKE: a computer program for earthquake response analysis of horizontally layered sites. *Technical Report EERC 72/12*, Earthquake Engineering Research Center, Berkeley, USA.
- [38] Aboye SA, Andrus RD, Ravichandran N, Bhuiyan AH, Harman N (2015): Seismic site factors and design response spectra based on conditions in Charleston, South Carolina. *Earthq. Spectra*, **31** (2), 723-744.
- [39] Anderson JG, Lee Y, Zeng Y, Day S (1996): Control of strong motion by the upper 30 meters. *Bull. Seismol. Soc. Am.*, **86** (6), 1749-1759.
- [40] Wakamatsu K, Matsuoka M (2006): Development of the 7.5-arc-second engineering geomorphologic classification database and its application to seismic microzoning. *Bull. Earthq. Inst. Univ. Tokyo*, **81**, 317-324.
- [41] Wald DJ, Allent TI (2007): Topographic slope as a proxy for seismic site conditions and amplification. *Bull. Seismol. Soc. Am.*, **97** (5), 1379-1395.